# Developing a Novel 1D-HAM Numerical Modelling Tool for Assessing the Hygrothermal Properties of Cross-Laminated Timber (CLT) Including Adhesive Layers


**Y. Vyas, D. Johns, R. Richman, and Z. Liao**

## 1 Introduction

Although developed in the early 1990s, mass timber has only begun to gain popularity as a viable and sustainable construction material in North America over the past decade [11]. Mass timber is a category of engineered wood products that can be used as the primary structure in mid- to high-rise buildings. Cross-laminated timber (CLT), a type of mass timber material, is composed of lumber laid and glued orthogonally. CLT can be used in floor, wall and roof assemblies to separate indoor and outdoor environments. Due to the hygroscopic properties of wood [6], CLT is highly susceptible to moisture and temperature fluctuations [3, 13]. During construction and service of CLT, elevated moisture content can cause material degradation through biological deterioration, dimensional instability and physical deterioration [12, 15, 19].

During the design phase of a CLT assembly or component, computer modelling can be used to measure the hygrothermal performance of the material based on variations of exterior and interior climate conditions. A hygrothermal model accounts for heat, air, and moisture (HAM) transfer. HAM modeling tools have been developed for hygrothermal analysis utilizing commercial finite element solvers to solve the governing ordinary differential equations of hygrothermal transport [2, 4, 14].

Y. Vyas (✉) · D. Johns · R. Richman · Z. Liao
Building Science, Department of Architectural Science, Ryerson University, Toronto, Canada
e-mail: yash.p.vyas@ryerson.ca

D. Johns
e-mail: dorothy.johns@ryerson.ca

R. Richman
e-mail: richman@ryerson.ca

Z. Liao
e-mail: zliao@ryerson.ca



S. Walbridge et al. (eds.), *Proceedings of the Canadian Society of Civil Engineering Annual Conference 2021*, Lecture Notes in Civil Engineering 248,
https://doi.org/10.1007/978-981-19-1004-3_36

Compared to experimental methods, validated numerical modeling is low cost, time-saving and has great predictability and controllability. Based on heat and mass conservation, governing equations of the hygrothermal modelling tool can be solved using various numerical methods, e.g. finite difference, finite volume, and finite element methods [7]. The HAM models are generally well defined for a static observation, however become much more complex under dynamic conditions [4, 5, 9, 16]. Established software such as DELPHIN, WUFI, and hygIRC, are generally used to conduct transient hygrothermal simulations. Although all of these softwares have been widely used for hygrothermal modelling, when it comes to CLT they overlook the impact of adhesive layers on air and moisture transport. These softwares use only average thermal and moisture resistance properties of the entire CLT material rather than treating the material as separate layers with distinct properties defining wood versus adhesive layers. Dividing the hygrothermal analysis into the actual layers of CLT will improve the accuracy of the analysis by indicating the varied moisture contents in each individual layer of wood as it is influenced by adjacent adhesive layers.

The requirement to specifically consider adhesive layers in CLT leads to the development of a novel lumped 1D ODE model using Matlab and Simulink. The main advantages of ODE lumped models include but are not limited to: (1) faster simulation time, (2) a larger control over the mesh parameters, and (3) increase in model applicability and adaptability based on various sample sizes. The model developed in this study is capable of simulating transient HAM transfer through the building enclosure, simplified solar radiation loads at the exterior boundary condition and simplified internal heat loads at the interior boundary condition. These capabilities are validated using existing hygrothermal softwares as described in the following research methodology.

This study aims to analyze the impact of adhesive layers in 3-layer and 5-layer CLT only. All material properties will be consistent between simulations except the number of wood layers and number of adhesive layers. In order to provide reliable results, base case conditions of 3-layer and 5-layer CLT will first be simulated without adhesive layers and results will be analyzed against identical CLT simulation results from WUFI. This establishes the accuracy and reliability of the 1-D HAM modelling tool developed. Subsequently, adhesive layers and their thermal and moisture-related properties will be added to the 1-D HAM modelling tool. Simulation results from the 1-D HAM modelling tool with adhesive layers are compared to simulation results from 1-D HAM modelling tool without adhesive layers in order to determine the impact of adhesive layers on the thermal and moisture processes and properties of the CLT. The quantity and validity of the results in this study establishes a reliable foundation for custom CLT simulations utilizing the adaptability and flexibility of the 1-D HAM modelling tool.

It is understood that the impact of adhesive layers on heat transfer will be negligible, however, based on the properties of the adhesives used in CLT manufacturing, as well as the primers required for adhesive application, it is anticipated that adhesive layers are likely to have a significant impact on moisture and air transfer through the CLT. It should be noted that due to the one-dimensional nature of the lumped model

developed, edge-glued vs. non-edge glued CLT does not impact the results of the developed model's simulations.

## 2 HAM Model Development

### *2.1 Theoretical Background*

Governing 1D HAM equations can be used to model the heat, air, and moisture transfer through an envelope assembly. All of the HAM equations are related to one another and impact the overall simulation results via internal dependency. To develop the 1D model, Matlab and Simulink were used. The tool developed is based on a lumped parameter model where the entire material, or slice of material, has one temperature and one moisture content.

The numerical model is based on finite volume analysis, where each node represents the centre of a volume, which can also be referred to as layer or slice. The thermal and moisture capacity and resistance of each material is based on the material properties (thermal capacity, thermal conductivity, moisture storage, vapour permeance and moisture suction pressure). Each layer is influenced by adjacent layers, as there is constant thermal and moisture transfer between layers due to variations in temperature and relative humidity between the indoor and outdoor environment. Figure 1 is a visual representation of the thermal transfer between a four-layer assembly, where the electrical current is analogous to heat transfer. The resistance between the two nodes can be referred to as thermal resistance and the capacitor at each node is analogous to the thermal capacity.

For this study, 3-layer and 5-layer CLT material is modelled with independent wood and adhesive layer nodes. As the wood material has a much higher moisture permeance than adhesive layers, each wood layer needed to be subdivided into two layers, in order to increase the accuracy of the model. Therefore a 3-layer CLT material will have six wood layers and two adhesive lateral layers; whereas, a 5-layer CLT material will have ten wood layers and four adhesive layers, as shown in Fig. 2.

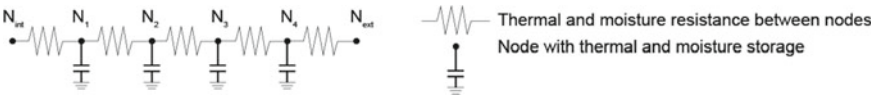


**Fig. 1** Diagram of thermal and moisture transfer in a 4-layer assembly

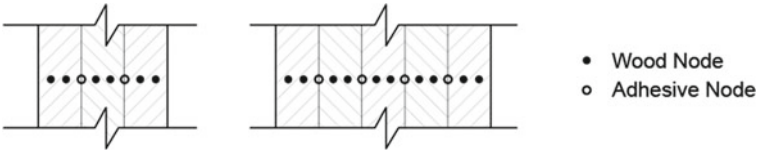


**Fig. 2** Diagram of 3-layer and 5-layer CLT node configurations

## *2.2 Heat Transfer*

The European standard CSN EN15026 evaluates the energy balance of a material using Fourier's law of heat transfer in one dimension where heat flux is a function of specific heat capacity, the density of the dry material and the temperature change. Fourier's law simplifies to Eq. 1, where: q is heat flux density ($W/m^2$), $C_p$ is specific heat capacity (J/kg K), $\rho_S$ is density ($kg/m^3$), and T is temperature (K).

$$-\frac{\partial q}{\partial x} = C_P \rho_S \frac{\partial T}{\partial t} \tag{1}$$

To simulate the overall heat transfer equation each material layer must be modelled, this includes the conduction, or heat flow, through each material. In addition to conduction, convection at the interior and exterior surfaces must also be accounted for [9, 17]. Finally, the exterior and interior surface nodes are also subject to additional temperature loads from solar radiation and internal factors.

### 2.2.1 Conduction

In general, the fundamental heat flow relationship was first defined by Fourier as expressed in Eq. 2 [20], where: q is heat flow (W/mK), k is thermal conductivity (W/mk), and T is temperature (K or °C).

$$q = -k * \text{grad}T \tag{2}$$

This is more commonly expressed as shown in Eq. 3, where: Q is heat flow rate (W), U is thermal transmittance ($W/m^2K$), A is area ($m^2$), and T is temperature (K or °C).

$$Q = U*A*\Delta T \tag{3}$$

Conduction was modelled in Simulink as expressed in Eq. 4, where: Q is heat flow rate (W), A is area ($m^2$), T is temperature (K or °C), l is material thickness (m), and k is material thermal conductivity (W/mK).

$$q = \frac{A^* \Delta T}{(1/k)} \tag{4}$$

It should be noted that for each node of the model to be represented in the centre of each material layer, the resistances from the materials on either side of the current layer must be averaged with the current layer's resistance. For example, if node 2 is being modelled, Eq. 5 would be used where: R12 and R23 are the calculated average thermal resistances from either side of the node of the material. See Fig. 1 for node configuration and heat and moisture resistance visualization.

$$R_{12} = \frac{(R_1 + R_2)}{2} \quad \& \quad R_{23} = \frac{(R_2 + R_3)}{2} \tag{5}$$

R12 and R23 are then used to calculate $q_{in}$ and $q_{out}$ for the energy balance of the node—in this case, node 2. For the temperature of the node to be calculated, $q_{total}$ for that node must be divided by the heat capacity of that node, which is a product of the material's density, specific heat capacity and volume, and integrated with an initial temperature value (set to a constant of 20 °C at each node). Note that the initial temperature does not impact the overall energy balance, it simply provides a starting point at which to begin energy balancing of each material layer.

### 2.2.2 Boundary Conditions

Convection must be accounted for at both the exterior and interior sides of a building assembly [9, 14, 17]. Convection is proportional to the temperature difference and can be expressed in Newton's Law of Cooling as shown in Eq. 6, where: Q is heat flow rate (W), $h_c$ is convective heat transfer coefficient ($W/m^2K$), A is surface area ($m^2$), $T_S$ is surface temperature (K or °C), and $T_o$ is atmospheric temperature (K or °C).

$$Q = h_c * A * (T_S - T_o) \tag{6}$$

Equation 6 is used for both interior and exterior surface film coefficients, however, the convective heat transfer coefficient ($h_c$) at the exterior surface must also account for air velocity [20] as expressed in Eq. 7, where: V is air velocity (m/s).

$$h_c = 5.6 + 3.9 * V \tag{7}$$

In addition to the convective forces at the exterior surface, there is also significant heat gain at the exterior surface of an assembly due to solar radiation [9, 10]. Solar radiation must consider the surface emissivity, the angle of the assembly, and the temperature difference between the exterior atmosphere and the surface. The relationship of these factors as modelled are expressed in Eq. 8, where: $q_{solar}$ is solar heat flux ($W/m^2$), FE is the emissivity factor, FA is the angle factor, and $\sigma$ is the

Stephen-Boltzmann constant ($5.67 \times 10^{-8}$ W/m$^2$K$^4$).

$$q_{solar} = F_E * F_A * \sigma * \left(T_s^4 - T_a^4\right) \tag{8}$$

The Simulink model accounted for all of these factors as they influence solar radiation using the combined Eq. 9, where: $Q_{solar}$ is the total solar radiation (W), A is the surface area (m$^2$), $\alpha$ is the material absorptance, $i_{sw}$ is the incident shortwave radiation, $\varepsilon$ sky is the emissivity of the sky, $\varepsilon$ surface is the emissivity of the surface, FA is the angle factor, and $\sigma$ is the Stephen-Boltzmann constant ($5.67 \times 10^{-8}$ W/m$^2$K$^4$) [20].

$$Q_{solar} = A\left[(\alpha * i_{sw}) + \left(F_A * \varepsilon_{sky} * \sigma * T_a^4\right) - \left(F_A * \varepsilon_{surface} * \sigma * T_s^4\right)\right] \tag{9}$$

In addition to the convective forces at the interior surface, there is also heat gain at the interior surface due to occupancy conditions including people, lighting and equipment loads [10]. These internal gains were accumulated as expressed in Eq. 10, where: $Q_{internal}$ is the internal gain in energy (W), #people is the number of people in the space, $E_{person}$ is the energy per person (W/person), A is the floor area (m$^2$), Lighting Load is as stated (W/m$^2$), and Equipment Load is as stated (W).

$$Q_{internal} = \left(\#people * E_{person}\right) + (A * \text{Lighting Load}) + (\text{Equipment Load}) \tag{10}$$

Cumulatively, the relationship between Eqs. 4–10 were modelled in Simulink in order to simulate heat transfer through the specified material assembly. See Fig. 4 showing both assemblies and their node configurations.

## 2.3 *Moisture Transfer*

In order to simulate moisture transfer in an assembly, the Simulink model has accounted for vapour diffusion, advection and liquid transfer, this is expressed in Eq. 11, where: $g_v$ is the vapour mass flux (kg/m$^3$s), $g_a$ is advection mass flux (kg/m$^3$s), $g_l$ is liquid mass flux (kg/m$^3$s), and w is moisture content (kg/m$^3$s).

$$\frac{\partial w(\varphi)}{\partial t} = -\nabla g_v - \nabla g_a - \nabla g_l \tag{11}$$

### 2.3.1 Vapour Diffusion

The diffusion flux of a material can be calculated using Fick's law [20]. In Fick's law, the partial vapour pressure is a function of temperature and vapour pressure difference, as expressed in Eq. 12, where: $g_v$ is the vapour mass flux (kg/m$^3$s),

$\delta_{material}$ is the permeability of the material (ng/Pa m s), and $P_V$ is the vapour pressure (Pa).

$$g_v = -\delta_{material}(\varphi) P_v(T, \varphi) \tag{12}$$

This is commonly described as expressed in Eq. 13, where: $q_v$ is vapour flux (ng/m$^2$s), M is the vapour permeance (ng/Pa m$^2$s), and $P_V$ is the vapour pressure (Pa).

$$q_v = -M\Delta P_v \tag{13}$$

Vapour diffusion was modelled in Simulink as expressed in Eq. 14, where: $Q_v$ is the vapour flow rate (ng/s), $\mu$ is the vapour permeability (ng/Pa m s), $P_V$ is the vapour permeance (Pa), A is the surface area (m$^2$), and l is the thickness of the material (m).

$$Q_v = \frac{-A\Delta P_v}{\left(\frac{l}{\mu}\right)} \tag{14}$$

It should be noted that in order for each node of the model to be represented in the centre of each material layer as required and illustrated in Fig. 3, the vapour resistances of the materials on either side of the current layer must be averaged with the current layer's resistance. For example, if node 2 is being modelled, Eq. 15 would be used, where: $RV_{12}$ and $RV_{23}$ are the average vapour resistances at either side of node 2 (Pa m$^2$s/ng).

$$RV_{12} = \frac{RV_1 + RV_2}{2} \quad \& \quad RV_{23} = \frac{RV_2 + RV_3}{2} \tag{15}$$

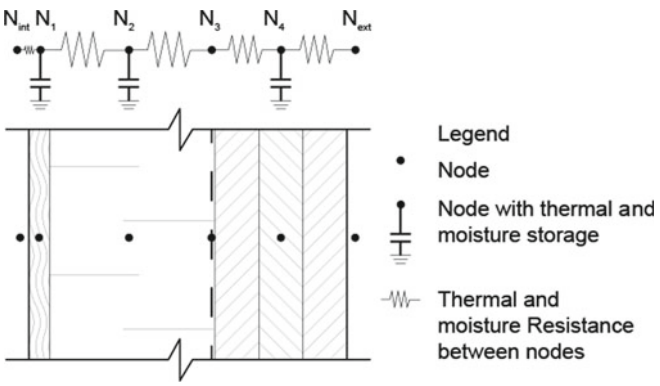


**Fig. 3** Diagram of node configuration in calibration model for validation with WUFI

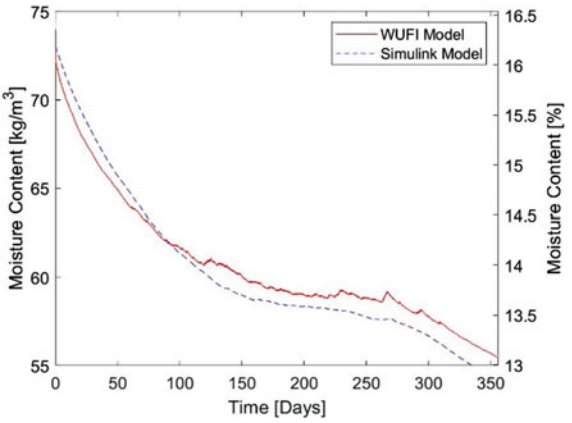


**Fig. 4** Validated temperature, relative humidity and moisture content results of 1D-ODE HAM model using WUFI

$RV_{12}$ and $RV_{23}$ must then be used to calculate $q_{Vin}$ and $q_{Vout}$ for the moisture balance of the node—in this case, node 2. In order for the vapour diffusion of the node to be calculated, the $q_{Vtotal}$ for that node must be divided by the moisture capacity of that node, which is a product of the material's density, water vapour capacity and volume, and integrated with an initial relative humidity (RH) value (set to a constant of 80% RH at each node). Note that the initial RH does not impact the overall mass balance, it simply provides a starting point at which to begin the mass balancing of each material layer.

### 2.3.2 Advection

The advection mass flux can be calculated by water vapour content in the air multiplied by the ratio of air water vapour permeability and water vapour permeability of material [2, 20], as shown in Eq. 16. Where, $g_a$ is advection mass flux [kg/m$^3$ s], $\rho_v$ is density of water vapour content of air or humidity by volume [kg/m$^3$], and $\mu$ is μ-factor is the vapor resistance factor which is the ratio between air vapour permeability and material vapour permeability.

$$g_a = \rho_v(T, \varphi)\mu \tag{16}$$

### 2.3.3 Liquid Transfer

Liquid transfer, also described as capillary suction flux, can be calculated using Darcy's law which is a product of liquid water permeability and suction pressure [20]. The liquid water transfer can be calculated through Eq. 17, where $g_l$ is liquid mass flux (kg/m$^3$s), $K_l$ is liquid water permeability of materials (kg/m$^3$ s Pa), and suction pressure (Pa).

$$g_l = -K_l(\varphi)P_{suc} \tag{17}$$

## 3 Model Simulation and Validation

A sample 1 m × 1 m wall assembly was modelled to evaluate the hygrothermal performance of the CLT in the Simulink model. The sample wall assembly is composed of the following materials (from exterior to interior): wood cladding, XPS insulation, vapour permeable air barrier, and CLT. The inclusion of an air space has been negated due to its negligible effects on heat and moisture transfer. The wall assembly remained consistent for each simulation except for the properties of the CLT which vary according to the comparative analysis described in Sect. 4. To analyze the hygrothermal impact of the adhesive layers in CLT only, all CLT wood layers have been modelled uniformly to be 40 mm thick. The material characteristics inputted into the numerical model (i.e. thermal conductivity, vapour permeability, moisture sorption curve and suction pressure) were gathered directly from WUFI in order to maintain analogous characteristics for validation of the numerical model. Material RH values were modelled to begin at 80% RH to be conservative in terms of construction and service RH levels and in order to perceive initial drying behaviour. Interior temperatures and relative humidities were modelled at 20 °C and 40% RH in winter and 24 °C and 60% RH in summer. The climate conditions were based on the Typical Meteorological Year (TMY) 2 dataset in Toronto, ON. Based on literature reviewed [1, 18], a 2-dimensional crack-flow analysis, as well as a sensitivity analysis conducted comparing Simulink and WUFI results, the air change per hour (ACH) is assumed to be 1 ACH.

The primary model validation was conducted without accounting for adhesive layers. The results of temperature and moisture content at the centre of the CLT were compared with an identical WUFI simulation. Since the baseline model was accurate, the more detailed model was developed using adhesive layers.

Figure 4 compares the temperature, relative humidity and moisture content results from the single CLT node, as illustrated in Fig. 3, between the WUFI simulation and the 1D-ODE HAM model simulation. The results are within an acceptable range therefore validating the 1D-ODE HAM model for additional simulations including adhesive layers as well as increased wood layer nodes. These additional layers and nodes, as illustrated in Fig. 5, decrease the granularity and increase the accuracy of the results; they also provide additional outputs throughout the layers of CLT for further analysis.

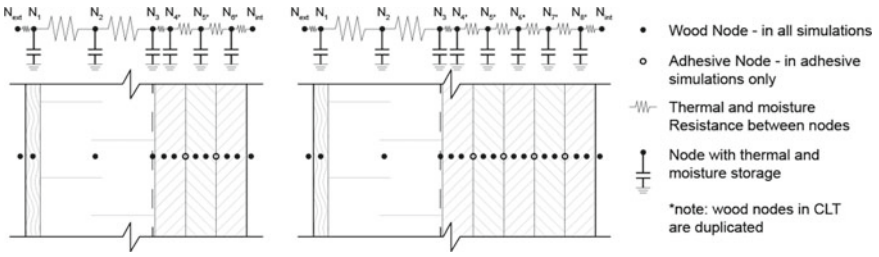


**Fig. 5** Node configuration in 3-layer CLT and 5-layer CLT assemblies with and without adhesive layers

## 4 Comparative Results of CLT with and Without Adhesive Layers

In order to analyze the impact of the adhesive layers on moisture transport in both 3-layer and 5-layer CLT, the node distribution throughout the CLT is critical. Figure 5 shows the distribution of nodes within the wall assembly incorporating 3-layer CLT and in the wall assembly incorporating 5-layer CLT, both assuming the inclusion of adhesive layers.

Figures 6 and 7 show the temperature in the two nodes of the centre layer of wood (see Fig. 5) in 3-layer CLT and 5-layer CLT respectively. As hypothesized, Figs. 6 and 7 confirm that the adhesive layers have no impact on the thermal resistance of CLT, hence the dashed lines (without adhesive) do not differ from the solid lines (with adhesive). Figures 8, 9, 10 and 11 show the impact of adhesive layers on moisture transport in 3-layer and 5-layer CLT, effectively determining the effect the adhesive layers have on the hygrothermal performance of CLT.

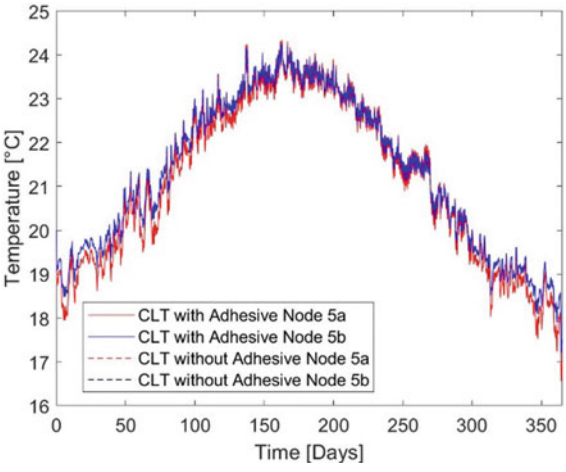


**Fig. 6** Temperature in centre wood nodes of 3-layer CLT with and without adhesive layers

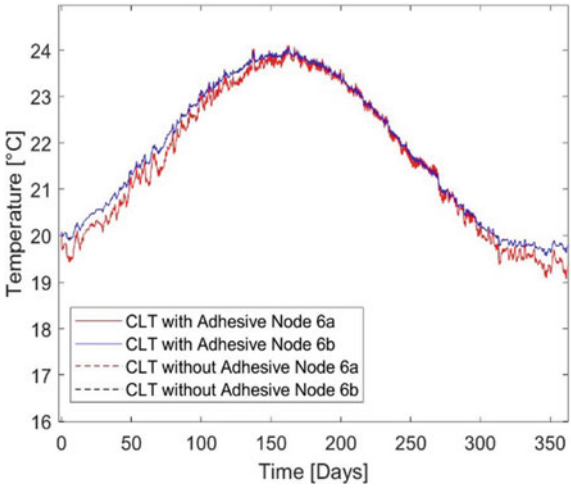


**Fig. 7** Temperature in centre wood nodes of 5-layer CLT with and without adhesive layers

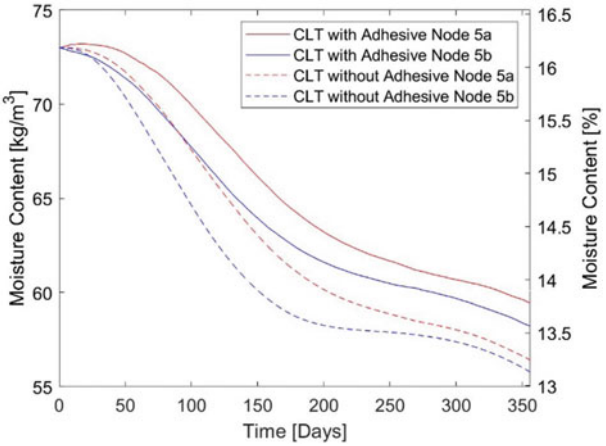


**Fig. 8** Moisture content in centre wood nodes of 3-layer CLT with and without adhesive layers

Figures 8 and 9 show the moisture content in the two nodes of the centre layer of wood (see Fig. 5) in 3-layer CLT and 5-layer CLT respectively. Comparing nodes in the same location within the depth of either CLT layup (e.g. CLT with adhesive Node 2a vs. CLT without adhesive Node 2a) illustrates the relatively higher moisture content (MC) in nodes within CLT including adhesive layers during the time period (single year) simulated. Figures 8 and 9 therefore confirm that, as expected, the adhesive layers do slow the rate of moisture transfer through the CLT. The comparisons plotted above also illustrate the magnitude of the influence adhesives have on slowing the drying rate of the CLT from a relatively high MC of approximately 16.5%. Over

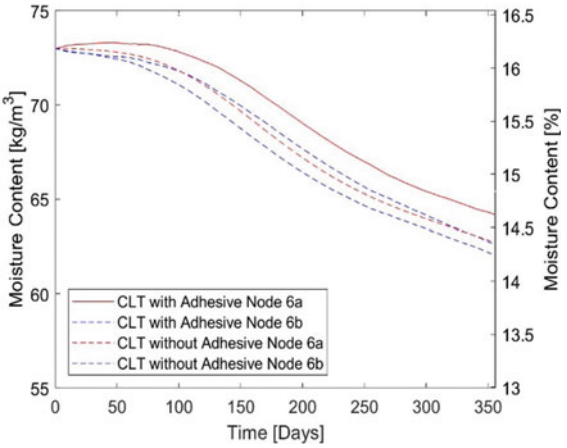


**Fig. 9** Moisture content in centre wood nodes of 5-layer CLT with and without adhesive layers

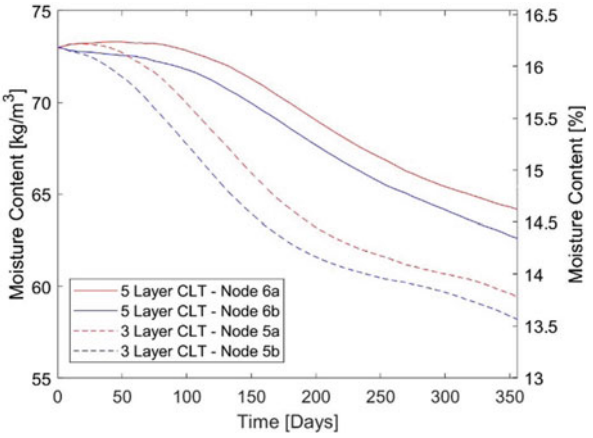


**Fig. 10** Moisture content in centre wood nodes of 3-layer versus 5-layer CLT without adhesive layers

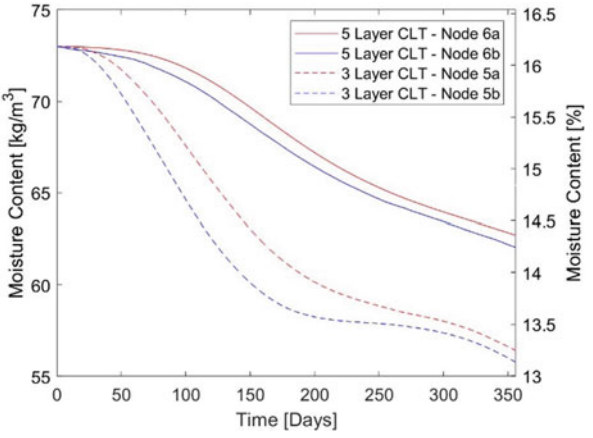


**Fig. 11** Moisture content in centre wood nodes of 3-layer versus 5-layer CLT with adhesive layers

a longer period of time, it is anticipated that the adhesives would impact the moisture uptake rate in a similar manner and that the magnitude would fluctuate as the centre and adjacent nodes approach equilibrium moisture content (EMC).

Figures 10 and 11 compare the moisture content of the centre two wood nodes in 3-layer versus 5-layer CLT without (Fig. 10) and with (Fig. 11) adhesive layers, effectively comparing the impact of additional wood and adhesive layers on the MC of the centre wood nodes. It is evident from the plots, that the middle layer of wood in the 5-layer CLT has a slower drying rate than in the middle layer of wood in the 3-layer CLT, therefore indicating that the additional wood layers on either side of the middle nodes in the 5-layer CLT slow the rate of moisture transfer through the CLT. Furthermore, the results confirm there is also a slower change in moisture content in wood layers in the simulations which include adhesive layers.

From the results of these simulations, it is anticipated that over a longer period of time, the middle layer of wood in 5-layer CLT would be exposed to fewer and slower moisture fluctuations than the middle layer of wood in 3-layer CLT. It can also be anticipated that the magnitude of impact on the moisture transfer would increase as the number of wood and adhesives layers increase, however, the relationship may not be linear.

## 5 Conclusions and Future Research

The results of the simulations performed in this study, show that the adhesive layers in CLT have no impact on the thermal performance of the material. However, the adhesive layers show a significant impact on the moisture resistance of the material. Therefore, including adhesive layers as discrete components in hygrothermal simulations of CLT is necessary to determine the moisture content in each wood layer (node) of the material. This in turn, also improves the accuracy of predicting moisture-related degradation through biological deterioration, dimensional instability, and physical deterioration.

The flexibility of the 1D-ODE HAM modelling tool developed in this study enables the input of exact envelope material characteristics as well as specific indoor and outdoor climatic conditions, as illustrated in the simulations conducted by [8]. Additionally, the modelling tool also enables the simulation of assemblies incorporating CLT with higher levels of accuracy than existing hygrothermal software which applies homogenous hygrothermal properties to CLT.

Future research will include laboratory and field testing to further validate and improve the overall accuracy of the numerical model. Future laboratory and field testing will also enable further research involving moisture transfer processes in CLT as they relate specifically to air tightness, defined boundary conditions, and varied climate conditions.

## References


1. ASHRAE (2017) ASHRAE Standard 90.1–2019. Energy standard for buildings except low-rise residential buildings. American Society of Heating, Refrigerating, and Air-Conditioning Engineers, Inc., Atlanta, GA
2. Belleudy C, Woloszyn M, Chhay M, Cosnier M (2016) A 2D model for coupled heat, air, and moisture transfer through porous media in contact with air channels. Int J Heat Mass Transf 95(April):453–465. https://doi.org/10.1016/j.ijheatmasstransfer.2015.12.030
3. Brischke C, Meyer L, Bornemann T (2013) The potential of moisture content measurements for testing the durability of timber products. Wood Sci Technol 47(4):869–886. https://doi.org/10.1007/s00226-013-0548-5
4. Chung D, Wen J, James Lo L (2020) Development and verification of the open source platform, HAM-tools, for hygrothermal performance simulation of buildings using a stochastic approach. Build Simul 13(3):497–514. https://doi.org/10.1007/s12273-019-0594-5
5. De Rosa M, Bianco V, Scarpa F, Tagliafico LA (2014) Heating and cooling building energy demand evaluation; a simplified model and a modified degree days approach. https://doi.org/10.1016/j.apenergy.2014.04.067
6. FPL (2010) Wood handbook, wood as an engineering material, Centennial. Forest Products Library, Madison, WI
7. James WL (1998) Electric moisture meters for wood. US For Prod Lab Res Pap
8. Johns D, Vyas Y, Richman RC, Liao Z (2021) Hygrothermal analysis of CLT in Canadian climates with and without adhesive layers using a 1D-HAM numerical modelling tool. In: CSCE 2021 annual conference materials specialty conference
9. Kalagasidis AS, Hagentoft C (2002) Simulink modelling tool for HAM system analyses in building physics. In: 6th symposium on building physics in the Nordic countries
10. Kalagasidis AS, Weitzmann P, Nielsen TR, Peuhkuri R, Hagentoft CE, Rode C (2007) The international building physics toolbox in simulink. Energy Build 39(6):665–674. https://doi.org/10.1016/j.enbuild.2006.10.007
11. Karacabeyli E, Douglas B (2013) CLT: handbook cross-laminated timber
12. Karacabeyli E, Gagnon S (2019) Canadian CLT handbook, Volume 1: 2019 edn. National Library of Canada, Pointe-Claire, QC
13. Kordziel S, Glass SV, Boardman CR, Munson RA, Zelinka SL, Pei S, Tabares-Velasco PC (2020) Hygrothermal characterization and modeling of cross-laminated timber in the building envelope. Build Environ 177(June):106866. https://doi.org/10.1016/j.buildenv.2020.106866
14. Li Q (2008) Development of a hygrothermal simulation tool (HAM-BE) for building envelope study. Concordia University
15. McClung R (2013) Field study of hygrothermal performance of cross-laminated timber wall assemblies with built-in moisture. Ryerson University
16. Nicolae A, Iordache V (2012) Modelling and simulation of HAM processes. Acta Technica Napocensis: Civil Eng Architect 55(3). http://constructii.utcluj.ro/ActaCivilEng/download/atn/ATN2012(3)_1.pdf
17. Qin M, Belarbi R, Aït-Mokhtar A, Nilsson L-O (2008) Simultaneous heat and moisture transport in porous building materials: evaluation of nonisothermal moisture transport properties. J Mater Sci 43(10):3655–3663. https://doi.org/10.1007/s10853-008-2584-3
18. Richman RC, Pressnail KD (2009) A more sustainable curtain wall system: analytical modeling of the solar dynamic buffer zone (SDBZ) curtain wall. Build Environ 44(1):1–10. https://doi.org/10.1016/j.buildenv.2008.01.006
19. Singh T, Page D, Simpson I (2019) Manufactured structural timber building materials and their durability. Constr Build Mater 217(August):84–92. https://doi.org/10.1016/j.conbuildmat.2019.05.036
20. Straube JF, Burnett EFP (2005) Building science for building enclosures. Building Science Press Inc., Westford, MA